Neutron scattering and the critical behavior of the three-dimensional Ising antiferromagnet FeF_2

D. P. Belanger
Department of Physics, University of California, Santa Cruz, California 95064
and Department of Physics, Brookhaven National Laboratory, Upton, New York 11973

H. Yoshizawa*
Department of Physics, Brookhaven National Laboratory, Upton, New York 11973
(Received 4 August 1986)

Neutron scattering has been used to study a high-quality single crystal of the very anisotropic antiferromagnet FeF_2 over the reduced temperature range $10^{-4} < |t| < 10^{-1}$. Analysis of the data by use of the Lorentzian scattering form of Ornstein and Zernike is shown to be inadequate, particularly for $T < T_c$. The use of better theoretical scattering forms for $|t| < 10^{-2}$ yields power-law behavior with the exponents $\nu = 0.64 \pm 0.01$ and $\gamma = 1.25 \pm 0.02$ and the amplitude ratios $\kappa_0^+/\kappa_0^- = 0.53 \pm 0.01$ and $\kappa_0^+/\kappa_0^- = 4.6 \pm 0.2$ for the inverse correlation length and staggered susceptibility, respectively. These results are in excellent agreement with the theory for the three-dimensional Ising model. Hence, the consistency between theory and neutron scattering in FeF_2 is greatly improved over previous experiments.

INTRODUCTION

Neutron-scattering techniques have long been used to characterize the critical behavior of magnetic crystals.[1] We have used an excellent quality single crystal of FeF_2, which is a particularly good three-dimensional ($d=3$) Ising antiferromagnet, to obtain the critical exponents and amplitude ratios for the correlation length ξ and the staggered susceptibility χ_s. Not only do we find critical parameters consistent with theory, but also demonstrate that the traditionally used Lorentzian form for the $\mathbf{q}$-dependent susceptibility $\chi(\mathbf{q})$ is inadequate for analysis of the scattering data for reduced temperatures $|t| = |T/T_c - 1| < 10^{-3}$. Power-law behavior for ξ and χ_s is observed when the more accurate expressions for $\chi(\mathbf{q})$ introduced by Fisher and Burford[2] for $T > T_c$ and by Tarko and Fisher[3] for $T < T_c$ are used in the analysis.

It has been shown in a similar study[4] for a $d=2$ Ising system that the Lorentzian form for $\chi(\mathbf{q})$ is inadequate for characterizing the critical scattering. Unlike the present case, the correct form for $\chi(\mathbf{q})$ can be calculated[5] for $d=2$.

In the quasielastic approximation,[1,6] which is good in very anisotropic crystals such as FeF_2, the scattering intensity is proportional to

$$S(\mathbf{q},T) = \sum_{\mathbf{r}} e^{i\mathbf{q}\cdot\mathbf{r}} S(\mathbf{r},T) = \langle \mathbf{s}_{-\mathbf{q}} \cdot \mathbf{s}_{\mathbf{q}} \rangle \ , \tag{1}$$

where $S(\mathbf{r},T) = \langle \mathbf{s}_0 \cdot \mathbf{s}_{\mathbf{r}} \rangle$ is the two-spin correlation function and $\mathbf{q}$ is the reduced lattice vector. For a pure, translationally invariant antiferromagnetic crystal,

$$\langle \mathbf{s}_{-\mathbf{q}} \cdot \mathbf{s}_{\mathbf{q}} \rangle = \chi(\mathbf{q}) + m_s^2 \delta(\mathbf{q}) \ , \tag{2}$$

where $m_s \sim |t|^{\beta}$ is the staggered magnetization. Scaling theory predicts[7]

$$\chi(\mathbf{r},T) \sim r^{-d+2-\eta} D(r/\xi) \ , \tag{3}$$

where $\xi = \xi_0^{\pm} |t|^{-\nu}$ and ξ_0^+ (ξ_0^-) is the amplitude for $T > T_c$ ($T < T_c$). This is equivalent to the scaling relation

$$\chi(\mathbf{q}) = A\kappa^{2-\eta} D(q/\kappa) \ , \tag{4}$$

with

$$\kappa = 1/\xi = \kappa_0^{\pm} |t|^{\nu} \ . \tag{5}$$

Above the upper critical dimension $d_u = 4$, for short-range interactions, $\eta = 0$ and $\chi(\mathbf{q})$ is given by the particularly simple Lorentzian form

$$\chi(\mathbf{q}) = \frac{A}{q^2 + \kappa^2} \ . \tag{6}$$

At the physically realizable dimensions $d=2$ and 3, $\chi(\mathbf{q})$ must deviate from the Lorentzian form to satisfy scaling with $\eta > 0$. A commonly used modification is

$$\chi(\mathbf{q}) = \frac{A_0 \kappa^{\eta}}{q^2 + \kappa^2} \ , \tag{7}$$

which satisfies the requirement

$$\chi_s = \chi(0) = \chi_0^{\pm} |t|^{-\gamma} \ , \tag{8}$$

with $\gamma = \nu(2-\eta)$. In practice, the scattering data for a given temperature are often fitted using Eq. (6). The exponent and amplitude ratio for χ_s are then obtained by fitting A/κ^2 to Eq. (8), with the implicit assumption that $A = A_0 \kappa^{\eta}$. As we shall show, this procedure is not adequate for $|t| < 10^{-3}$ in FeF_2, and we must use more accurate approximations.

For $T > T_c$ the expression

$$\chi(\mathbf{q}) = A^+ \kappa^{-2+\eta} \frac{(1 + \phi^2 q^2/\kappa^2)^{\eta/2}}{1 + \psi q^2/\kappa^2} \tag{9}$$

has been developed by Fisher and Burford[2] (FB), which satisfies scaling and is believed to be accurate for experi-

TABLE I. Parameter values used for data analysis with Eqs. (9) and (10).

η	$\frac{1}{18}=0.056$
ϕ	0.15
ψ	$1+1/2\eta\phi^2=1.001$
σ	$2\eta=0.111$
ϕ'	0.3247
ϕ''	0.093 55
ψ'	$1+1/2\eta\phi'^2+\sigma(\phi'^2-\phi''^2)=1.0137$

mentally accessible $\mathbf{q}$ and t. For $T<T_c$ we have the complementary form

$$\chi(\mathbf{q})=A^-\kappa^{-2+\eta}\frac{(1+\phi'^2q^2/\kappa^2)^{\sigma+\eta/2}}{(1+\psi'q^2/\kappa^2)(1+\phi''^2q^2/\kappa^2)^{\sigma}}\ , \tag{10}$$

as introduced by Tarko and Fisher (TF).[3]

The parameters[8] in Eqs. (9) and (10) are listed in Table I. For continuity as κ goes to zero, we must have

$$A=A^+\phi^\eta/\psi=A^-\phi'^{2\sigma+\eta}\psi'\phi''^{2\sigma}\ . \tag{11}$$

We shall see presently that these expressions are sufficient for analyzing the scattering line shapes. The parameters κ and A obtained in this way yield critical behavior for ξ and χ_s consistent with the theory of the $d=3$ Ising model for $10^{-4}<|t|<10^{-2}$.

Our use of the anisotropic antiferromagnet FeF_2 has been particularly motivated by recent scattering studies of the random-exchange[9] (RE) and random-field[10] (RF) Ising models using the randomly dilute $Fe_xZn_{1-x}F_2$ system. The very Ising-like character of FeF_2 is a result of a very strong single-ion anisotropy.[11] For reduced temperatures $|t|<2\times10^{-2}$, it exhibits specific-heat critical behavior that agrees extremely well with theory.[12] However, the critical exponents for ξ and χ_s determined in a previous neutron-scattering experiment are not in satisfactory agreement with present theory. Hutchings *et al.*[13] obtained the earlier results $\nu=0.67\pm0.04$ and $\gamma=1.38\pm0.08$ for $T>T_c$ and $\nu'=0.7\pm0.2$ and $\gamma'=1.6\pm0.2$ for $T<T_c$. Several theoretical results for exponents are given in Table II. The theoretical values are consistent with each other, although quite different techniques were used. The disagreement between theory and experiment and the large error values for the experimental show the experiment to be an inadequate test of the $d=3$ Ising model. Similarly, the amplitude ratios found in earlier scattering experiments,[13] $\kappa_0^+/\kappa_0^-=0.43\pm0.11$ and $\chi_0^+/\chi_0^-=6.1\pm1.0$, agree with the theoretical ratios shown in Table III only because of the very large errors associated with the experimental values. Since the scaling requirements $\nu=\nu'$ and $\gamma=\gamma'$ were not imposed in the experimental analysis, the amplitude ratios are slightly ambiguous.

Before delving into detailed investigations of critical scattering in the random $Fe_xZn_{1-x}F_2$ system, it is crucial to resolve the discrepancies between the early scattering critical parameters for pure FeF_2 and those from the present theory of the $d=3$ Ising model. In addition, large non-Lorentzian contributions to the scattering line shapes are expected in the dilute systems.[14,15] It is therefore prudent to understand the non-Lorentzian effects in pure FeF_2 before attempting to investigate the details of critical scattering in the RE and RF Ising model systems.

EXPERIMENTAL DETAILS

The scattering measurements were made at the Brookhaven High Flux Beam Reactor using a two-axis spectrometer configuration. For data very close to T_c the beam was collimated horizontally to 10′ of arc before the

TABLE II. Theoretical exponents for the $d=3$ Ising model (adapted from footnote h) obtained from high-temperature (HT), field-theoretic (FT), Monte Carlo (MC), and scaling-field (SF) techniques.

	ν	γ	η	Ref.
HT	0.6305±0.0015	1.2385±0.0025	0.035 ±0.003	a
		1.2385±0.0015		b
	0.6300±0.0015	1.237 ±0.002	0.0359±0.007	c
FT	0.630 ±0.0015	1.241 ±0.002	0.031 ±0.004	d
	0.630 ±0.002	1.241 ±0.004	0.031 ±0.011	e
	0.628 ±0.001		0.035 ±0.002	f
MC	0.629 ±0.004		0.031 ±0.005	g
SF	0.626 ±0.009	1.23 ±0.02	0.040 ±0.007	h

[a]J. Zinn-Justin, J. Phys. (Paris) **42**, 783 (1981).
[b]J. H. Chen, M. E. Fisher, and B. G. Nickel, Phys. Rev. Lett. **48**, 630 (1982).
[c]B. G. Nickel and J. J. Rehr (unpublished).
[d]J. C. le Guillou and J. Zinn-Justin, Phys. Rev. B **21**, 3976 (1980).
[e]G. A. Baker, Jr., B. G. Nickel, and D. I. Meiron, Phys. Rev. B **17**, 1365 (1978).
[f]S. G. Gorishny, S. A. Larin, and F. V. Tkachov, Phys. Lett. **101A**, 120 (1984).
[g]G.S. Pawley, R. H. Swendsen, D. J. Wallace, and K. G. Wilson, Phys. Rev. B **29**, 4030 (1984).
[h]K. E. Newman and E. K. Riedel, Phys. Rev. B **30**, 6615 (1984).

TABLE III. Theoretical values for the amplitude ratios for the $d=3$ Ising Model.

κ_0^+/κ_0^-	κ_0^-	χ_0^+/χ_0^-	Ref.
0.524		4.8	a
0.510±0.008	0.89	5.10±0.05	b

[a]E. Brézin, J. C. le Guillou, and J. Zinn-Justin, Phys. Lett. **47A**, 285 (1974).
[b]H. B. Tarko and M. E. Fisher, Phys. Rev. B **11**, 1217 (1975).

pyrolytic graphite monochromator, between the monochromator and sample, and between the sample and detector. For data further from T_c, where κ is larger than about 0.01 RLU, 20′ collimation was used throughout to increase the scattering intensity. Two pyrolytic graphite filters were used to reduce higher-order neutrons. The incident wave vector was 2.58 Å^{-1}.

The FeF_2 sample is the same one used in the linear birefringence measurements of the specific heat.[12] It is in the shape of a right parallelepiped of dimensions $4\times4\times6$ mm^3. The c axis is perpendicular to the long axis of the sample. The sample was mounted on a copper holder with the c axis in the horizontal plane. Cadmium was used to mask the copper near the sample. A heater coil and thermistor were mounted on the copper holder for temperature control and measurement.

The thermistor was calibrated during the experiment using a commercially calibrated platinum thermometer also mounted in the holder. The sample was in a He atmosphere inside a sealed aluminum can. This arrangement allowed better than 1 mK temperature control using liquid nitrogen as the coolant.

The lattice parameters of FeF_2 were measured to be $a=b=4.70$ Å and $c=3.31$ Å. For best resolution, all measurements of the critical behavior were made in transverse scans about the (100) magnetic reflection. The magnetic Bragg scattering at (100) for $T<T_c$ is, in principle, represented by the δ function in Eq. (2). For good quality single crystals the Bragg peak is broadened only by the spectrometer's limited resolution. We have determined the spectrometer resolution by scanning the Bragg peak at a temperature $T=69.8$ K, which is much less than $T_c=78.4$ K, so that fluctuation-scattering contributions are negligible. Since the FeF_2 crystal used is of such high quality, the observed amplitude of the Bragg scattering does not increase with m_s^2 for $T\ll T_c$, as indicated in Eq. (2). This effect, known as extinction, is a result of the strong scattering in the first part of the crystal. This depletes the beam and reduces the scattering from the remaining part of the crystal. Extinction is a property only of the crystal and the scattering remains well described by a δ function, albeit with a smaller amplitude. Extinction cannot influence the observed line shape of the Bragg scattering, which is only determined by the instrumental resolution. For quasielastic scattering in $d=3$ systems the resolution centered at (100) can be represented[1] quite well as an ellipsoid in reciprocal space with its principal axes along the transverse $(1\,q\,0)$, longitudinal $(1+\eta\,0\,0)$, and vertical $(1\,0\,\xi)$ directions. In Fig. 1 we

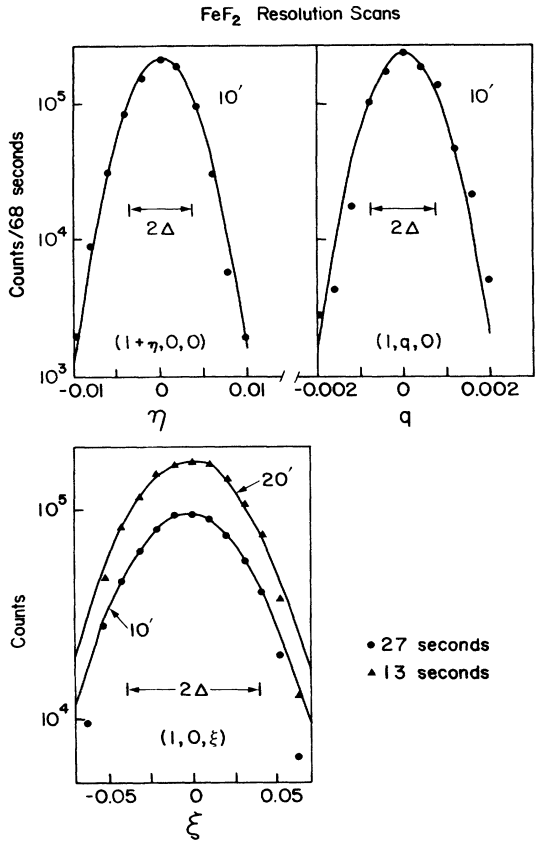

FIG. 1. Instrumental resolution measurements of the (100) magnetic Bragg peak at $T=69.8$ K in the longitudinal, transverse, and vertical directions for 10′ collimation and in the vertical directions for 20′ collimation.

show the three measured resolution scans for 10′ vertical collimation and for the vertical direction for 20′. The transverse and longitudinal scans for 20′ are very similar in shape to those for 10′, but with larger widths. Because the sample is of high quality, the resolution scans for 10′ collimation are quite well described by Gaussian functions, shown by the solid curves in Fig. 1, with half widths at half maximum (HWHM's) of 0.000 75, 0.0037, and 0.039 RLU (reciprocal-lattice units) for the transverse, longitudinal, and vertical scans, respectively. The corresponding widths for 20′ collimation are 0.0016, 0.0075, and 0.039 RLU, respectively.

CORRECTIONS FOR INSTRUMENTAL RESOLUTION

The significant resolution widths, necessary for sufficient neutron intensity, require that substantial corrections be made to the theoretical line shapes before fitting to the data. The finite instrumental resolution must be folded into $S(\mathbf{q},T)$ either by employing Gaussian approximations to the measured resolution line shapes or by performing the necessary integrations numerically, using the data directly from the experimental resolution scans.

In the first case for transverse scans, a good approximation to the scattering intensity is

$$I(\mathbf{q})=I_0\Delta_t\Delta_l\Delta_v\Pi^{3/2}\int_{-\infty}^{\infty}\int_{-\infty}^{\infty}\int_{-\infty}^{\infty} da\,db\,dc\,S((q-q_0-a)^2+b^2+c^2)\exp\left[-\left[\frac{(q-q_0-a)^2}{\Delta_t^2}+\frac{b^2}{\Delta_1^2}+\frac{c^2}{\Delta_v^2}\right]\right]+B\ , \tag{12}$$

where I_0 is a constant which depends upon the experimental configuration and incident neutron flux, Δ_t, Δ_l, and Δ_v are the Gaussian Bragg-peak widths ($1.201\times$HWHM) for the transverse, longitudinal, and vertical directions, respectively, q_0 is a parameter to be fitted to account for slight misalignment of the sample and detector angles, and B is a small background term to be fitted for each scan which allows for neutron counts not associated with the diverging longitudinal susceptibility. In the second case we have, to a good approximation,

$$I(\mathbf{q})=I_0\frac{\sum_a\sum_b\sum_c S((q-q_0-a)^2+b^2+c^2)T_{(a)}L_{(b)}V_{(c)}}{\sum_a\sum_b\sum_c T_{(a)}L_{(b)}V_{(c)}}+B\ , \tag{13}$$

where T, L, and V are the resolution functions in the transverse, longitudinal, and vertical directions, respectively, measured at equally spaced points, as is shown, for example, in Fig. 1.

In the least-squares analysis of the scattering data, we tried both of the techniques just described and found essentially identical results using the Lorentzian form for $S(\mathbf{q},T)$ in Eq. (6). For the more complicated FB and TF expressions in Eqs. (9) and (10), we found the summations to be more convenient. All of the results reported here were obtained using the latter technique.

The significant HWHM in the vertical direction makes comparison with small q ($q/\kappa\ll 1$) expansions, such as the one by Aharony and Fisher[12] for $T>T_c$, difficult. Even when the nominal spectrometer setting is for small q, the large vertical instrumental width allows a non-negligible scattering contribution from large reduced lattice vectors in the vertical direction. To use such expansions in small q, the vertical collimation would need to be much smaller. However, this would require a more intense neutron source for reasonable scattering intensity.

EXPERIMENTAL RESULTS

Two typical transverse scans at 10′ collimation for $T<T_c$ are shown in Fig. 2 along with fits to the TF equation with instrumental resolution folded in. Spurious background counts were 4 ± 2 counts/min for 10′ collimation. The data taken for very small $|q|$ are not shown since these contain magnetic Bragg-scattering contributions and were not used in the fit of the data to $\chi(\mathbf{q})$. In principle, one could study the Bragg scattering, which should be proportional to the square of the staggered magnetization, $m_s^2\sim|t|^{2\beta}$. Unfortunately, the very high quality of the sample leads to extinction effects which make comparison of the data to m_s^2 difficult in the present experiment. To eliminate the Bragg scattering from consideration, we only used data with $|q|$ much larger than the transverse resolution. For 10′ collimation we eliminated data with $|q|<0.005$ or larger and for 20′ collimation we eliminated the range with $|q|<0.01$ or larger. Data for $T>T_c$ were treated in a similar manner to avoid spurious multiple scattering which can appear at the magnetic Bragg point. All scans were taken out to $|q|=0.5$.

Nearly all of the nonlinear least-squares fits to the data yielded χ^2 in the range $1<\chi^2<2$. The fits to the FB and TF forms for $\chi(\mathbf{q})$ generally yielded χ^2 only slightly smaller (typically 10%) than the corresponding Lorentzian fits. With the necessarily large resolution corrections, it is extremely difficult to evaluate the appropriateness of the different theoretical forms of $\chi(\mathbf{q})$ directly from the quality of the fit to data taken at one temperature. However, by examining the behavior of the parameters A and κ as a function of reduced temperature, we can clearly demonstrate, especially from the results for $T<T_c$, that consistent critical behavior is not obtained using the Lorentzian expression for $|t|<10^{-3}$, but is seen for the FB and TF analysis.

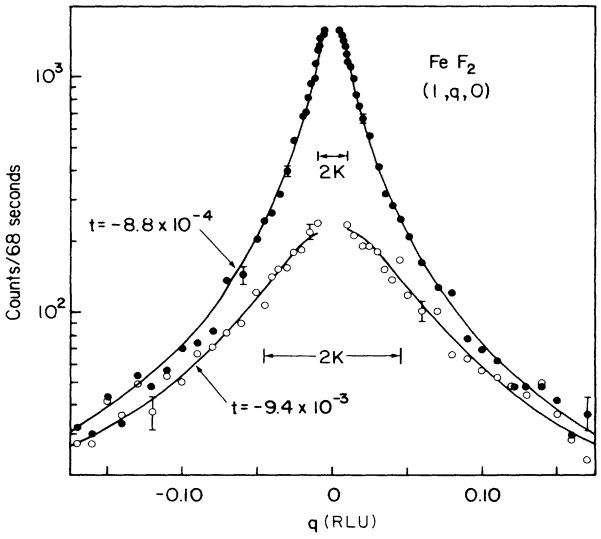

FIG. 2. Two transverse scans about the (100) Bragg point with 10′ collimation for $t=-8.8\times10^{-4}$ and -9.4×10^{-3}. The solid curves are best fits to the data using the TF line shape.

TABLE IV. Typical fits for $\kappa=\kappa_0^{\pm}|t|^{\nu}$. For FeF_2.

	$10^{-4}<\|t\|<10^{-2}$	$10^{-4}<\|t\|<10^{-1}$	$10^{-3}<1\|t\|<10^{-1}$
T_n	78.418±0.001	78.418±0.001	78.431±0.06
ν	0.64 ±0.01	0.65 ±0.01	0.66 ±0.01
κ_0^+/κ_0^-	0.53 ±0.01	0.54 ±0.01	0.56 ±0.01
κ_0^-	0.90 ±0.04	0.93 ±0.03	0.93 ±0.03

Figure 3 shows the logarithm of the effective κ obtained from Lorentzian fits of the data versus the logarithm of $|t|$. The errors quoted for values of the parameters obtained from fits to the data represent two standard deviations. However, they do not reflect systematic sources of error. Clear deviations from the expected power-law behavior are seen below $|t|=10^{-3}$, especially for $T<T_c$. Increasing the region of data eliminated around $q=0$ increases the deviation from power-law behavior for $T<T_c$. For $T>T_c$ the values of κ become rather indeterminate for small $|t|$ since κ is much smaller than $|q|$ for any the data being analyzed when the region $|q|<0.01$ is excluded. The solid straight lines in Fig. 3 are taken from the FB and TF analysis shown in Fig. 4. The solid and dashed curves are the results of computer simulations.[16] Simulated data were generated using the FB and TF equations with appropriate resolution effects and random noise added. The simulated data were then analyzed in the same manner as the experimental data using the Lorentzian line shape, yielding the curves shown in Fig. 3. The agreement between the analyses of the simulated and experimental data demonstrates that the observed deviation of κ from power-law behavior is due to the inadequacy of the Lorentzian approximation and not to any systematic error in the analysis of the experimental data.

The results for κ from the analysis of the scattering data using the FB and TF forms for $\chi(\mathbf{q})$ are shown in Fig. 4. κ appears to follow power-law behavior for $10^{-4}<|t|<10^{-1}$, as demonstrated by the solid lines, which are fits to Eq. (5). The results for small $|t|$ were obtained using data with $|q|>0.005$. Increasing the range of excluded data yields κ values consistent with the same power-law behavior but with increased error bars. From the behavior of κ vs $|t|$, it is quite evident that the FB and TF approximations are significant improvements over the commonly used Lorentzian-scattering line shape for $|t|<10^{-3}$, particularly for $T<T_c$. The small improvement in the results using the FB rather than the Lorentzian line shape does not warrant further comparisons with other comparable line shapes for $T>T_c$.[17]

Fitting the values of κ shown in Fig. 4 to Eq. (5) for the power-law behavior of the inverse correlation length, we obtain the critical exponent $\nu=0.64\pm0.01$ and the amplitude ratio $\kappa_0^+/\kappa_0^-=0.53\pm0.01$ for the range $10^{-4}<|t|<10^{-2}$. These values compare well with theory and fairly well with the values obtained using other ranges of reduced temperature, as is summarized in Table IV. In addition, the experimental value for the amplitude of the inverse correlation length, $\kappa_0^-=0.90\pm0.04$, for $10^{-4}<|t|<10^{-2}$, agrees well with the theoretical value[3]

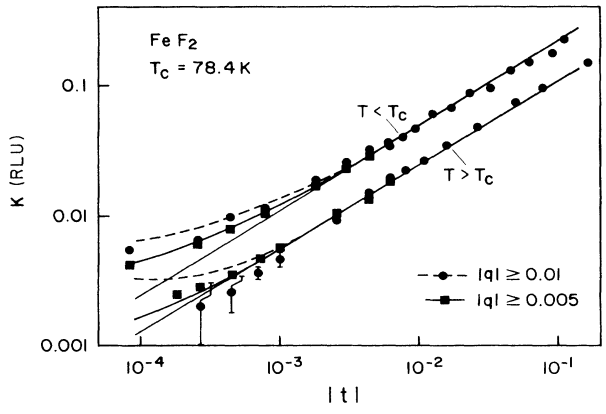

FIG. 3. The logarithm of κ, obtained using the Lorentzian line shape in Eq. (8), vs the logarithm of $|t|$. The data used in the analyses were for $|q|>q^{\min}$. For the solid squares $q^{\min}=0.005$, with the exceptions $t=-7.7\times10^{-3}$, -6.1×10^{-3}, and -4.4×10^{-3}, where $q^{\min}=0.008$, 0.007, and 0.006, respectively. For the solid circles $q^{\min}=0.01$, with the exceptions $t=-3.3\times10^{-2}$, -4.6×10^{-2}, -6.3×10^{-2}, -9.1×10^{-2}, and -1.1×10^{-1}, where $q^{\min}=0.02$, 0.02, 0.04, 0.04, and 0.08, respectively. The dashed and solid curves are from computer simulations briefly described in the text. The straight solid line is taken from Fig. 4.

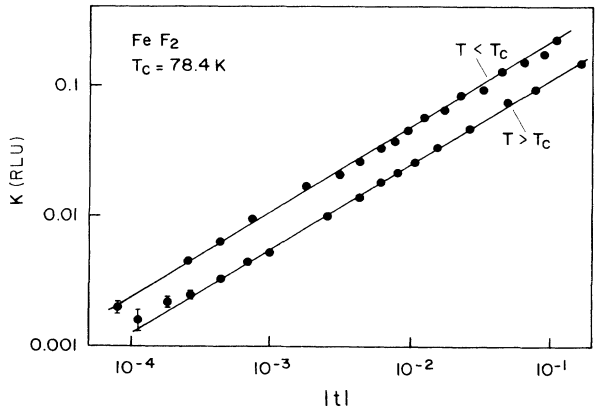

FIG. 4. The logarithm of κ, obtained using the FB ($T>T_c$) and TF ($T<T_c$) line shapes in Eqs. (9) and (10), vs the logarithm of $|t|$. Data were analyzed using $q^{\min}$ values corresponding to those in Fig. 3, taking the smaller $q^{\min}$ for solid squares when shown.

TABLE V. Typical fits for $\chi_s = A\kappa^{-2} = \chi_0^{\pm} |t|^{-\gamma} + B$. For FeF_2.

	$10^{-4} < \|t\| < 10^{-2}$	$10^{-4} < \|t\| < 10^{-1}$	$10^{-3} < \|t\| < 10^{-1}$
T_n	78.418±0.001	78.418±0.001	78.419±0.004
γ	1.25 ±0.02	1.26 ±0.01	1.27 ±0.02
χ_0^+/χ_0^-	4.6 ±0.2	4.6 ±0.1	4.5 ±0.2
χ_0^-	1.09 ±0.12	0.77 ±0.05	0.96 ±0.09
B	14 ±30	10 ±3	10 ±3
T_n	78.418±0.001	78.418±0.001	78.424±0.004
γ	1.26 ±0.001	1.24 ±0.01	1.23 ±0.01
χ_0^+/χ_0^-	4.5 ±0.1	4.3 ±0.1	4.1 ±0.2
χ_0^-	0.83 ±0.07	0.93 ±0.05	1.24 ±0.08
B[a]	0	0	0

[a]Fixed to zero.

for the body-centered-cubic lattice expressed in our units and adjusted for the body-centered-tetragonal lattice of FeF_2. The consistency of the value $\nu = 0.64 \pm 0.01$ for the range $10^{-4} < |t| < 10^{-2}$ can be tested with the hyperscaling relation $2 - \nu d - \alpha = 0$, using the measured specific-heat exponent $\alpha = 0.11 \pm 0.005$. We obtain the result $2 - \nu d - \alpha = -0.03 \pm 0.04$.

Since we apparently have good fits of the data to the FB and TF line shapes yielding accurate values for κ and $A^{\pm}$, we can, in principle, extrapolate to $\mathbf{q} = 0$, giving us $\chi_s = \chi(0) = A^{\pm}\kappa^{-2+\eta}$. The logarithm of $A^{\pm}\kappa^{-2+\eta}$ is plotted versus the logarithm of $|t|$ in Fig. 5. Since two experimental configurations with different collimations were used to obtain data, it is necessary to normalize the intensities. We did this by taking two scans at the same temperature, $t = 6 \times 10^{-3}$, one with 10′ and one with 20′ collimation. The scattering widths were identical, within error, and the amplitude ratio is used as a normalization factor for the amplitude A obtained at other temperatures with 20′ collimation. Power-law behavior is indeed observed for $10^{-4} < |t| < 10^{-2}$. A least-squares analysis of these values to Eq. (8) yields the exponent $\gamma = 1.25 \pm 0.02$ and the amplitude ratio $\chi_0^+/\chi_0^- = 4.6 \pm 0.2$. Again, these values agree very well with theory and with values obtained using other ranges of reduced temperature, as summarized in Table V. Fits were made with and without a constant-background term, which would account for regular terms in the staggered susceptibility. Only for $|t| > 3 \times 10^{-2}$ is there an obvious departure from power-law behavior in Fig. 5.

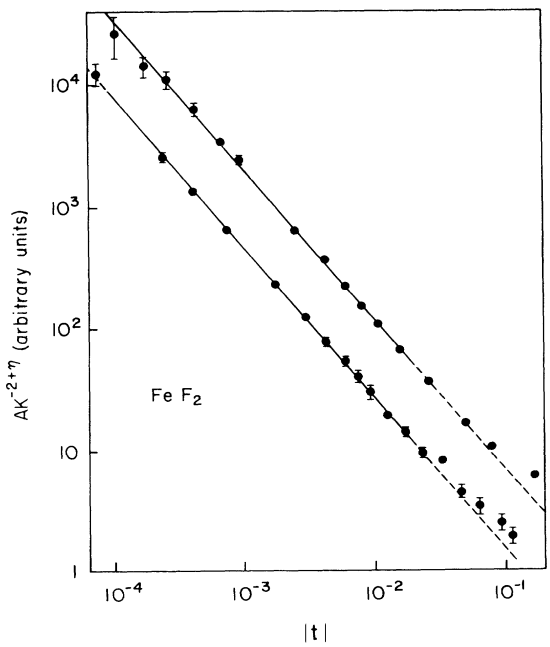

FIG. 5. The logarithm of $A^{\pm}\kappa^{-2+\eta}$ vs the logarithm of $|t|$, showing the power-law behavior of the staggered susceptibility. The solid lines represent the best fit to the data over the reduced temperature range $10^{-4} < |t| < 2 \times 10^{-2}$ and the dashed lines are extensions of the fit outside this range.

We may estimate the value of the exponent η from the scaling relation $\gamma = \nu(2 - \eta)$. From the values $\nu = 0.64 \pm 0.01$ and $\gamma = 1.25 \pm 0.02$ for the range $10^{-4} < |t| < 10^{-2}$, we obtain $\eta = 0.05 \pm 0.06$, consistent with theory (Table II), which predicts a small positive value.

The scattering amplitude A is generally not examined separately. However, in this study we found the behavior of A versus the logarithm of $|t|$, as shown in Fig. 6, to be a sensitive test of the appropriateness of the theoretical scattering function and a way to judge when departure from Ising critical behavior occurs. In the upper portion of Fig. 6 is the behavior of A as obtained using the FB and TF equations. For $3 \times 10^{-5} < |t| < 10^{-2}$, A is constant as expected, within 5%. For $|t| > 10^{-2}$, A sharply increases for both $T > T_c$ and $T < T_c$. The lower part of Fig. 6 shows the corresponding behavior for A when the Lorentzian line shape is used in the data analysis. For $T > T_c$ and $3 \times 10^{-5} < |t| < 10^{-2}$ the slow increase of A is consistent with the behavior $A = A_0\kappa^{\eta}$ with $\eta = 0.035$, a value consistent with theory. Instead of continuing this behavior, as would be the case if the values for A followed the dotted curve in Fig. 6, A increases sharply for $|t| > 10^{-2}$. For $T < T_c$ the behavior of A is inconsistent with $A = A_0\kappa^{\eta}$ since A decreases with $|t|$ until $|t| \approx 10^{-2}$, where A again sharply increases. The behavior below T_c demonstrates once again the inadequacy of the Lorentzian approximation in describing the scattering data. The rise in A for $|t| > 10^{-2}$ occurs where the system begins to crossover to Heisenberg be-

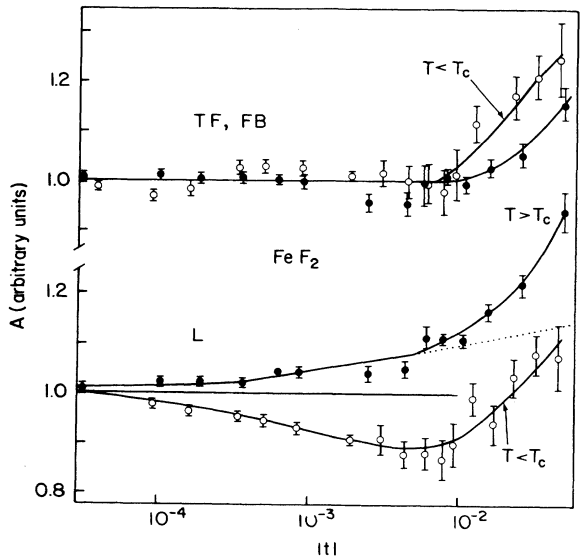

FIG. 6. The amplitude A vs the logarithm of $|t|$, obtained by fitting the data to the Lorentzian (L), TF, and FB scattering line shapes. For the L results above T_c, the solid curve for $|t|<10^{-2}$ is consistent with $\eta=0.035$.

havior and the description of the scattering in terms of purely Ising-like fluctuations is no longer appropriate. This is consistent with the specific-heat critical-behavior experiments on FeF_2,[12] where it was concluded that the asymptotic Ising region was for $|t|<2\times10^{-2}$. The most reliable exponents and amplitudes are therefore those obtained from fits to the data for $|t|<10^{-2}$. For completeness we have included examples of fits for other ranges of $|t|$ in Tables IV and V. Only slight changes in the critical parameters are obtained.

Attempts to include corrections to scaling in the fits for κ and χ_s were rather inconclusive. Although it is difficult to rule out completely the influence of correction-to-scaling terms on the exponents obtained for $10^{-4}<|t|<10^{-2}$, we suspect that any change in the exponents is very small. If this were not the case, then the critical parameters obtained from fits with no correction terms should show a much greater variation for larger $|t|$, where correction terms become more important.

CONCLUSION

We have shown that for precise determination of critical behavior in neutron-scattering experiments, it is necessary to use theoretical expressions for $\chi(\mathbf{q})$ which are more accurate than the simple Lorentzian often used to analyze scattering data. In the $d=3$ anisotropic antiferromagnet FeF_2 the Lorentzian form is inadequate for $|t|<10^{-3}$, its failure being especially apparent for $T<T_c$. The FB and TF approximations provide the necessary improvement for $10^{-4}<|t|<10^{-2}$. In this range critical exponents and amplitude ratios for ξ and χ_s are obtained which are in excellent agreement with theoretical values for the $d=3$ Ising model. Significant departure from the expected asymptotic $d=3$ Ising behavior is observed for $|t|>10^{-2}$, consistent with observations based on the behavior of the specific heat of FeF_2.

A similar neutron-scattering study[18] has been made previously using MnF_2, a system much like FeF_2, except for a much smaller anistropy. Specific-heat studies[12] show that the asymptotic Ising behavior in this system is only for $|t|<10^{-3}$. Ising-to-Heisenberg crossover effects should be correspondingly larger in MnF_2, introducing systematic errors into the determination of critical parameters. In addition, for systems with such small anistropy there is a non-negligible scattering contribution resulting from the transverse susceptibility even within the asymptotic critical region. To determine the critical behavior of the divergent longitudinal susceptibility, the nondivergent transverse component must be subtracted from the total scattering. Any procedure used to accomplish this unfortunately adds systematic error. In the case of the very anisotropic system FeF_2, the scattering contribution of the transverse component in the present measurements is, at most, about 5 counts/min close to T_c. This is quite negligible, as seen in Fig. 2, and has been absorbed into the background term in the fitting of the scans. FeF_2 is therefore a much more reliable system for experimental tests of the $d=3$ Ising model.

At the critical point the second-order phase transition from liquid to gast should also belong to the $d=3$ Ising universality class. Hence, the critical scattering in such systems should also exhibit non-Lorentzian line shapes. It has indeed been shown,[19] using light-scattering techniques for $T>T_c$, that in this case as well the Ornstein-Zernike approximation is inadequate to characterize the critical behavior.

Having established that FeF_2 is, in fact, a superb $d=3$ Ising-model system, detailed studies of critical behavior in the dilute systems $Fe_xZn_{1-x}F_2$ are given more credibility as tests of the random-exchange and random-field Ising models. In the dilute systems, however, precise theoretical expressions for $S(\mathbf{q})$ are lacking. It is important that such theory be developed, so that critical scattering data in these systems may be fully utilized to characterize their critical behavior.

The consequence of using the Lorentzian approximation to the scattering line shape in the $d=2$ Ising system are much more profound than in the present case, as expected.[4,5] In particular, for K_2CoF_4 the amplitude ratios $\kappa_0^+/\kappa_0^-=0.19\pm0.03$ and $\chi_0^+/\chi_0^-=53.4\pm5.5$ were obtained. When the appropriate form for $\chi(\mathbf{q})$ given by Tarko and Fisher[3] was used for the analysis, the ratios $\kappa_0^+/\kappa_0^-=0.54\pm0.13$ and $\chi_0^+/\chi_0^-=32.6\pm3.0$ were obtained, which are in much better agreement with the theoretical values $\kappa_0^+/\kappa_0^-=0.50$ and $\chi_0^+/\chi_0^-=37.33$.

ACKNOWLEDGMENTS

We would like to acknowledge R. Cowley, M. Hagen, V. Jaccarino, G. Shirane, and C. Tracy for helpful discussions. We thank V. Jaccarino for the use of the FeF_2 sample. Work at Brookhaven National Laboratory was supported by the Division of Materials Sciences, U. S. Department of Energy, under Contract No. DE-AC02-76CH00016. This work was also supported in part by the U. S.-Japan Coorperative Program on Neutron Scattering.

*Permanent address: Institute for Solid State Physics, University of Tokyo, Roppongi, Minato-ku, Tokyo 106, Japan.

[1]See, for example, J. Als-Nielsen, in *Phase Transitions and Critical Phenomena,* edited by C. Domb and M. S. Green (Academic, New York, 1976).

[2]M. E. Fisher and R. J. Burford, Phys. Rev. **156**, 583 (1967).

[3]H. B. Tarko and M. E. Fisher, Phys. Rev. B **11**, 1217 (1975).

[4]R. A. Cowley, M. Hagen, and D. P. Belanger, J. Phys. C **17**, 3763 (1984).

[5]C. A. Tracy and B. McCoy, Phys. Rev. B **12**, 368 (1975).

[6]See, for example, S. W. Lovesay, *Theory of Neutron Scattering from Condensed Matter* (Clarendon, Oxford, 1984).

[7]M. E. Fisher, Rev. Mod. Phys. **46**, 597 (1974).

[8]The κ in Eqs. (9) and (10) refers to the inverse second-moment correlation length, which differs slightly from the true inverse correlation length. Hence, all experimental results also correspond to the second-moment correlation length.

[9]D. P. Belanger, A. R. King, and V. Jaccarino, Phys. Rev. B **34**, 452 (1986); R. J. Birgeneau, R. A. Cowley, G. Shirane, H. Yoshizawa, D. P. Belanger, A. R. King, and V. Jaccarino, *ibid.* **27**, 6747 (1983).

[10]D. P. Belanger, A. R. King, and V. Jaccarino, Phys. Rev. B **31**, 4538 (1985).

[11]M. T. Hutchings, B. D. Rainford, and H. J. Guggenheim, J. Phys. C **3**, 307 (1970).

[12]D. P. Belanger, P. Nordblad, A. R. King, V. Jaccarino, L. Lundgren, and O. Beckman, J. Magn. Magn. Mater. **31-34** , 1095 (1983).

[13]M. T. Hutchings, M. P. Schulhof, and H. J. Guggenheim, Phys. Rev. B **5**, 154 (1972).

[14]R. A. Pelcovits and A. Aharony, Phys. Rev. B **31**, 350 (1985).

[15]M. Schwarz and A. Soffer, Phys. Rev. B **33**, 2059 (1986).

[16]D. P. Belanger, M. L. Setliff, and D. M. Stone (unpublished).

[17]See, for example, A. J. Bray, Phys. Rev. B **14**, 1248 (1976).

[18]M. P. Schulhof, P. Heller, R. Nathans, and A. Linz, Phys. Rev. B **1**, 2304 (1970).

[19]R. F. Chang, H. Burstyn, and J. V. Sengers, Phys. Rev. A **19**, 866 (1979).